COMBUSTION AND FLAME 72: 159–173 (1988)

Assessment of a Partial-Equilibrium/Monte Carlo Model for Turbulent Syngas Flames

S. M. CORREA and A. GULATI

General Electric Company, Corporate Research and Development Center, Schenectady, NY 12309

and

S. B. POPE

Cornell University, Ithaca, NY 14853

Calculations and data for a turbulent jet flame of 40% CO, 30% H_2, and 30% N_2 in coflowing air are compared extensively. The calculations are based on a partial-equilibrium model for the oxyhydrogen radical pool including CO, and on a velocity–composition joint probability density function (pdf), which closes the turbulent flux and mean chemical source terms. The pdf is joint between the three velocity components and two thermochemical scalars needed to describe partial-equilibrium conditions. The equation is solved numerically by a Monte Carlo technique. The data used are major species concentrations and temperature from pulsed Raman scattering. Difficulties with Raman measurements at high temperatures and of measuring CO_2 directly are discussed. The Raman signals are taken from previous studies but here are corrected for high-temperature effects and CO_2 vibrational spectra. Temperatures are obtained from the instantaneous density of the major species rather than from the Stokes/anti-Stokes ratio, which is more affected by chemiluminescence. The level of agreement between the model and the data is more favorable to the partial-equilibrium model than previously thought. The relative simplicity of the partial-equilibrium model makes it a candidate for practical calculations.

INTRODUCTION

Although the fast chemistry or "mixed-is-burned" model for combustion is useful for understanding the gross aerodynamics in many combustion systems, there is an increasingly important range of phenomena that cannot be so accounted for. For example, finite-rate radical pool chemistry has been shown to be very influential in thermal NO_x and CO emissions from atmospheric H_2 and CO/H_2 flames [1] and to degrade combustion efficiency in supersonic combustion systems [2]. Localized effects including extinction due to turbulent stretching may be largely due to the chemistry not being fast compared with the turbulent microscales [3], as has been demonstrated in laminar CH_4 flames [4]. High-altitude limitations on aircraft combustors are caused in part by slow kinetics due to the low densities. It seems clear that as the limits of combustion equipment are expanded, it is more and more important to account for finite-rate chemical kinetics. On the other hand, detailed chemical kinetic mechanisms have been established only for the combustion of relatively simple fuels such as H_2, CO/H_2, and CH_4 [5]. The combustion of complex hydrocarbons of practical significance is usually represented by a semiempirical first step to simple constituents such as CO and H_2, with subsequent oxidation of the latter [5]. This may compromise

Published by Elsevier Science Publishing Co., Inc.
52 Vanderbilt Avenue, New York, NY 10017

0010-2180/88/$03.50

the understanding of, for example, "prompt" NO_x which is formed via hydrocarbon fragments [6]; it also leaves only the relatively simple fuels as candidates for studies in turbulent flames, where significant uncertainties regarding the chemical mechanisms involved would compound the problem of turbulence–chemistry interaction.

Kinetic mechanisms for even the simple fuels are quite complicated. Hydrogen combustion in air involves at least eight species (H_2, O_2, H_2O, N_2, O, OH, H, HO_2, etc.) and associated reactions. Methane combustion involves about 30 species and 100 reactions [7]. These mechanisms add too many transport equations to kinetics models to be usable in other than laminar flame calculations. Even in laminar flames the mathematical stiffness of the resulting set of equations requires special numerical methods as shown by Miller et al. [7].

Simpler models of the chemical kinetics are required for turbulent flames, where closure of turbulent flux and chemical source terms would increase the difficulties caused by a large set of species. Such models can be formulated by sacrificing a complete description of the chemistry. Ignoring the details of ignition, a recognition that the two-body chain-branching reactions (which produce radicals) are much faster than the three-body radical recombination reactions (which terminate combustion) leads to plausible models for flame propagation and burnout. Such models have been used for turbulent nonpremixed ("diffusion") flames of H_2 [8] and CO/H_2 [9] mixtures in the Reynolds number range Re = 1000–10,000. The assumption that the two-body reactions are relatively fast is supported by the work of Warnatz [10] for temperatures above 1700K. This simplification allows a two-variable description of the H_2 flame in terms of the mixture fraction and either a reaction progress variable for the oxyhydrogen radical pool [8] or a perturbation variable for mole number [11]. Such models are called partial-equilibrium models because the two-body reactions are assumed to be in equilibrium.

Assuming that the reaction CO + OH = CO_2 + H is also fast extends the applicability of the partial equilibrium model to CO/H_2 flames. This approach has been used in studies of laminar ethylene–air flames by Fenimore and Moore [12] and of turbulent CO/H_2 flames by Correa et al. [9] and by Pope and Correa [13].

Pope and Correa [13] used a Monte Carlo method to solve a modeled transport equation for the joint pdf of the three components of velocity and the two thermochemical variables used in the partial-equilibrium model. In this approach scalar fluxes and chemical source terms are closed exactly, pressure-correlations are modeled at the level used in the second-order closure Reynolds-stress models, and intermittency is accounted for through conditional modeling. In the context of shear flows such as the jet flame, this description of the flowfield must be regarded as (statistically) very complete. Dropping the assumptions of pdf shape and gradient-diffusion closure are among the important improvements in this model compared with traditional models. A more precise assessment of the chemical model is therefore possible. A conclusion of the latter work [13] was that CO levels were underpredicted, which was taken as evidence of finite-rate CO chemistry.

Correa et al. [9] implemented the partial-equilibrium model described above in an assumed-shape pdf/gradient-diffusion methodology. The density-weighted average equations were closed with the $k\epsilon1$ turbulence model, assuming gradient-diffusion closure for all fluxes. Transport equations for the hydrodynamics, turbulence kinetic energy and dissipation rate, and the means and variances of the mixture fraction (ξ) and a reaction progress variable (η) were solved. Since the latter four equations constitute the lowest moments of the joint pdf $P(\xi, \eta; \boldsymbol{x})$ for the thermochemical variables, an additional assumption of the pdf shape parameterized in terms of these moments leads to the local pdf. Although this model is not as well-founded as the joint velocity–scalar(s) pdf/Monte Carlo model [13], the results were quantitatively similar. A significant prediction of the Monte Carlo model is a strong correlation between ξ and η which is ignored in the simpler model. Both indicated good agreement with data on mean OH concentrations, with the Monte Carlo model predicting rms OH concentration in closer agreement with the data. The similarity between the results, despite significant differences in the models implied that the combus-

tion mechanisms rather than the flow model should be examined in efforts to improve understanding of turbulent syngas flames.

An explicit kinetic step for CO chemistry has been explored by Correa [14] by introducing a third variable for the perturbations of CO from the levels when in partial equilibrium with the radical pool. The results differed only in the upstream portion of the flame; i.e., the CO reached partial equilibrium levels within 25 diameters. It should be noted that adding thermochemical variables is computationally undesirable and improved performance of the two-variable model would be most welcome.

Recently, the raw Raman data obtained earlier have been reanalyzed to account for high-temperature correction factors and CO_2 vibrational spectra as described below. The agreement between the model calculations and the corrected data is more favorable to the two-variable partial-equilibrium model. The purpose of this paper is to discuss the methodology used to reanalyze the Raman data and to assess the performance of the partial-equilibrium model in greater depth than done previously. For completeness, the thermochemical and turbulent flow models are reviewed briefly. Data on mean and rms OH concentrations are unaffected by the present work. The agreement with these data [9, 13] is powerful support for the partial-equilibrium model.

THERMOCHEMICAL MODEL

The same thermochemical model is used here as was used by Correa et al. [9] and Pope and Correa [13]. The kinetic mechanism adopted consists of five fast shuffle reactions (S1)–(S5), which are considered to be in partial equilibrium:

$$H + O_2 = OH + O, \tag{S1}$$

$$O + H_2 = OH + H, \tag{S2}$$

$$H_2 + OH = H_2O + H, \tag{S3}$$

$$2OH = H_2O + O, \tag{S4}$$

$$CO + OH = CO_2 + H; \tag{S5}$$

and the three-body recombination reactions (R1)–(R4):

$$H + OH + M \rightarrow H_2O + M, \tag{R1}$$

$$H + O + M \rightarrow OH + M, \tag{R2}$$

$$H + H + M \rightarrow H_2 + M, \tag{R3}$$

$$CO + O + M \rightarrow CO_2 + M, \tag{R4}$$

which are relatively slow at pressures on the order of an atmosphere. Janicka and Kollman [8] used the scheme without the shuffle reaction (S5) in their studies of turbulent hydrogen flames including thermal NO formation. Warnatz [10] demonstrated the validity of the partial-equilibrium scheme in H_2–N_2–O_2 systems at high temperatures. Kaskan [15] and Fenimore and Moore [12] used the same approach to describe the combustion of carbon monoxide in laminar flames. Bilger and Starner [16] also discussed the merits of this kinetic scheme for turbulent hydrocarbon flames and concluded that it would be applicable at temperatures above 1800–1900K, with reaction (S5) being the first to deviate from partial equilibrium.

Eleven quantities comprising nine species concentrations (O_2, H_2, N_2, CO, CO_2, H_2O, O, H, OH), the density, and the temperature are required to describe the instantaneous state of the system. To reduce the number of variables, a linear combination of mass fractions is used, as suggested by Dixon-Lewis et al. [17]:

$$Y_{H_2}^* = Y_{H_2} + \frac{1}{2}\frac{W_{H_2}}{W_{OH}} Y_{OH} + \frac{W_{H_2}}{W_O} Y_O + \frac{3}{2}\frac{W_{H_2}}{W_H} Y_H + \frac{W_{H_2}}{W_{CO}} Y_{CO}, \tag{1}$$

where Y_j and W_j are the mass fraction and molecular weight, respectively, of species j. The formation rate of $Y_{H_2}^*$ is independent of the shuffle reactions (S1)–(S5) and depends only on the rates of the recombination reactions (R1)–(R4) provided partial equilibrium is maintained.

The system can now be related to just two variables. The first is the mixture fraction, ξ,

$$\xi = \frac{Z_i - Z_i^a}{Z_i^f - Z_i^a} = \frac{h - h^a}{h^f - h^a}, \tag{2}$$

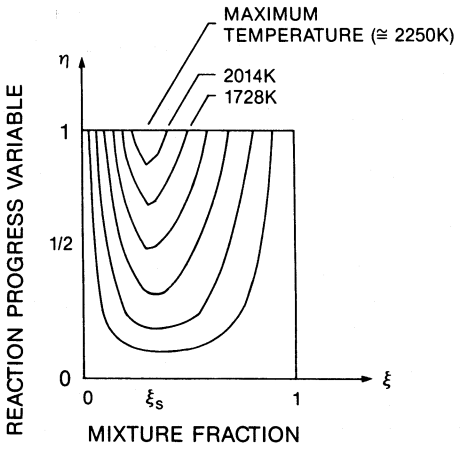

Fig. 1. Temperature contours in thermochemical space, taken from Correa et al. [9].

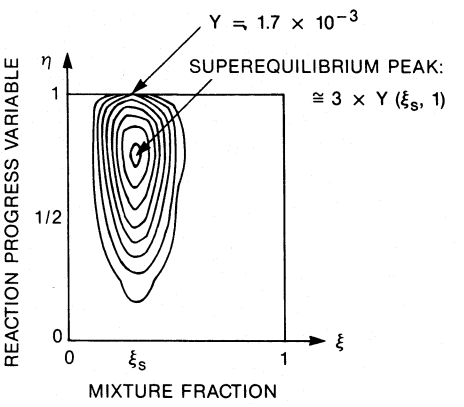

Fig. 2. OH contours in thermochemical space, taken from Correa et al. [9].

where Z_i is the atomic mass fraction of element i, h is the total (chemical plus sensible) enthalpy, and the superscripts a and f refer to air and fuel, respectively. ξ is the conserved scalar used in "fast chemistry" models. This approach is possible for flows at low Mach number because the local mechanical energy is not significant compared to the chemical and sensible enthalpy. The second variable is the reaction progress variable (η) defined by normalizing the variable $Y_{H_2}^*$ with its frozen ($Y_{H_2}^{*u}$) and equilibrium ($Y_{H_2}^{*e}$) values:

$$\eta = \frac{Y_{H_2}^* - Y_{H_2}^{*u}}{Y_{H_2}^{*e} - Y_{H_2}^{*u}} . \tag{3}$$

All the thermochemical variables can then be calculated for given ξ and η. Temperature and OH mass fraction contours (Figs. 1 and 2) show that the temperature decreases as η decreases from the equilibrium value of unity while OH has the expected superequilibrium peak [9]. Figure 2 also indicates that the degree of superequilibrium in OH ($[OH]_{max,\,\xi^*}/[OH]_{eqm,\,\xi^*}$) increases with deviation of ξ^* from stoichiometric, indicating that large superequilibrium effects can be present in rich or lean gas. Similar results are obtained for other radical species, although they could be more abundant on one side or the other of stoichiometric, e.g., H-atoms on the rich side. Effects on pollutant formation can be deduced from these figures. For example, contrary influences of superequilibrium on thermal nitric oxide are suggested by these calculations: with increasing superequilibrium (due to slow recombination reactions) O-atom levels increase while temperature decreases. Despite its exponential dependence on temperature, the NO formation rate increases. The effects of various diluents, via their efficiencies as third-body partners, on superequilibrium and thermal NO formation in turbulent jet flames have been discussed by Drake et al. [1].

The properties calculated above were stored in tabular form for use in the flow calculation. In addition to reducing the number of variables needed to describe combustion, the partial-equilibrium model reduces mathematical stiffness, since the fast (shuffle) reactions are not treated explicitly.

TURBULENT FLOW MODEL

The flow is described by the following dependent variables: velocity U, mixture fraction ξ, and reaction progress variable η. Here a one-point statistical description in terms of the joint pdf of U, ξ, and η is used. Since the flow is axisymmetric and statistically stationary, all one-point statistics depend only on the axial and radial coordinates, x and r. Being a one-point description, length-scale or time-scale information is not contained in the pdf and is, instead, supplied through a mixing-frequency model based on the local width of the shear layer.

The joint pdf $P(V, \tilde{\xi}, \tilde{\eta}; x, r)$ is the probability density of the simultaneous events $U = V$, $\xi = \tilde{\xi}$, and $\eta = \tilde{\eta}$ at that location in space and time. All one-point statistics are recovered from this pdf because the composition is a known function of ξ and η. For example, the mean of a quantity ϕ is

$$\langle \phi(x, r) \rangle \equiv \int\int_{\cdots} \phi(\tilde{\xi}, \tilde{\eta}) P(V, \tilde{\xi}, \tilde{\eta}; x, r) \cdot dv\, d\tilde{\xi}\, d\tilde{\eta}. \quad (4)$$

Any correlations such as higher moments or fluxes can be computed similarly. The problem is therefore to determine the joint pdf P at each point in the flowfield.

Pope [18] has developed a transport equation for the evolution of the joint pdf. An exact equation for P can be derived directly from the Navier–Stokes equations and the species conservation equations [19]. Even for variable-density flows with complex chemistry, convection (including all fluxes), chemical reaction, and the mean pressure gradient do not have to be modeled. Molecular transport and the fluctuating pressure gradient require modeling for closure. The modeling used here follows that of Pope [20] for a self-similar plane jet.

As discussed by Pope and Correa [13], a conditional model is used to discriminate between the turbulent and nonturbulent fluids. The mixture fraction ξ also is the concentration of nozzle fluid; hence $\xi = 0$ indicates nonturbulent ambient gas and $\xi > 0$ indicates turbulent gas.

Details of the stochastic mixing models, which account for molecular transport, and the stochastic reorientation model, which accounts for pressure fluctuation, are given by Pope [21] and Pope [19], respectively.

The mixing-frequency within the turbulent fluid cannot be generated in a one-point pdf model and so is supplied through the algebraic model,

$$\omega(x) = \omega^*(\tilde{u}(x, 0) - u_\infty)/(r_{0.9} - r_{0.1}). \quad (5)$$

Here ω^* is a dimensionless frequency constant taken to be 0.16 to match the measured spreading rate of the jet, $\tilde{u}$ is the mass-averaged velocity, and r_a is the radial position at which the mass-averaged excess velocity ratio has decayed to a. In jets such algebraic models for the mixing-frequency or length work well.

The pdf transport occurs in a multidimensional space composed of the independent variables in the problem, viz., two spatial variables, (x, r), three velocity variables V, and two scalar variables (ξ, η). Calculations of transport equations are already computationally strained in three dimensions and so a Monte Carlo numerical technique is used here [19]. As described by Pope and Correa [13], simplifications analogous to the boundary-layer approximation can be made in jet flows.

In the Monte Carlo method, the joint pdf is represented by a large number N of notional particles ($N \approx 35{,}000$). At location x, the nth particle has the radial position $r^{(n)}(x)$, velocity $U^{(u)}(x)$, and composition $\xi^{(n)}$, $\eta^{(n)}(x)$. Initial conditions are specified at the jet exit ($x = 0$). The measured initial conditions were not matched in detail, but care was taken to match the axial momentum and mixture fraction flow rates.

The solution was obtained for $0 \le x/d \le 100$ in a succession of 640 steps in x. In the general step from x to $x + \Delta x$ the particle properties ($r^{(n)}$, $U^{(n)}$, $\xi^{(n)}$, and $\eta^{(n)}$) evolve as described by Pope [19]. As a consequence of reaction, $\eta^{(n)}$ evolves for a time $\Delta x/U^{(n)}(x)$ according to the ordinary differential equation

$$\frac{d\eta^{(n)}}{dt} = w(\xi^{(n)}, \eta^{(n)}), \quad (6)$$

with the initial condition $\eta^{(n)}(x)$. A direct algorithm would require Eq. (6) to be integrated for each particle on each step, i.e., about 20 million times; instead, a computationally efficient table-lookup algorithm is used.

Mean quantities—either mass-averaged or volume-averaged—are extracted from the particle properties by cross-validated cubic smoothing splines.

RAMAN DATA REDUCTION

All the raw experimental data reported in this paper were previously obtained in the atmospheric pressure, subsonic, low-turbulence combustion

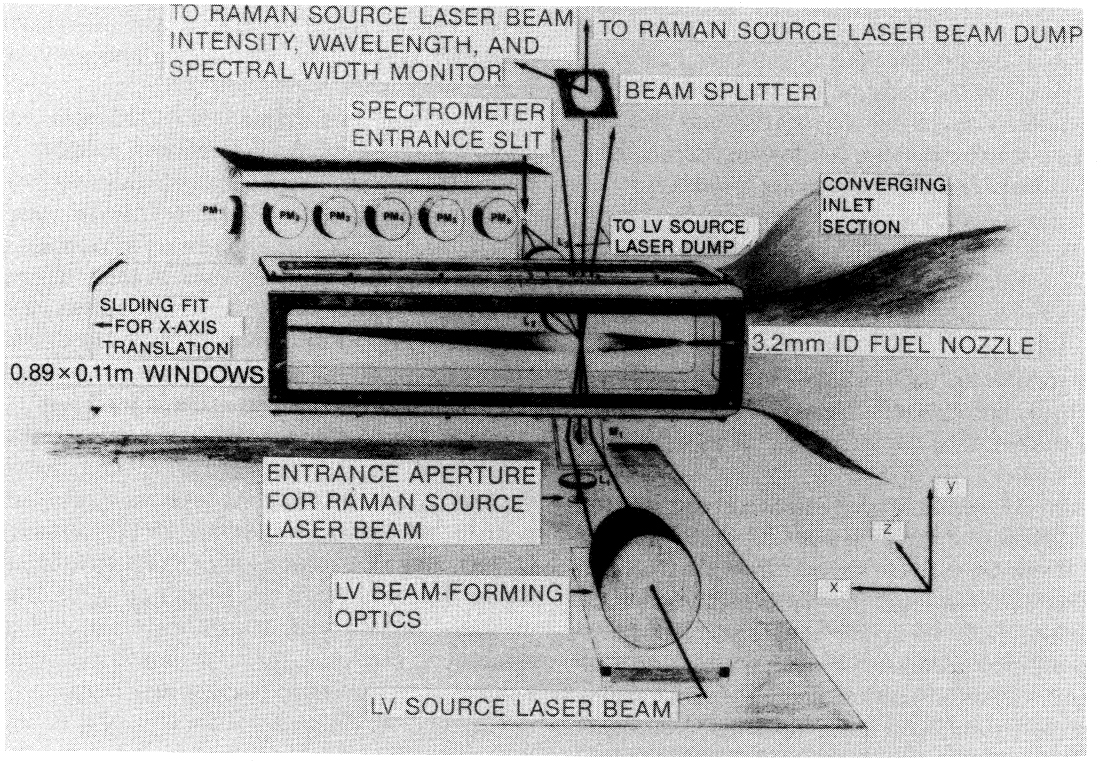

Fig. 3. Experimental setup showing the Raman apparatus.

test facility described in detail elsewhere [22]. The turbulent diffusion flame consists of a syngas fuel jet (30% H_2, 40%, CO, 30%, N_2) emerging from a nozzle of diameter $d = 3.18$ mm at an average velocity of 54.6 m/s, corresponding to a Reynolds number of 8500. The jet is surrounded by a coflowing air stream at a velocity of 2.4 m/s. The nonintrusive laser-based techniques used consist of pulsed Raman scattering for measurement of temperature and mole fractions of major species and laser-induced saturated fluorescence for measurement of OH concentration. Both these techniques have been discussed in detail [22–25]. Here the most pertinent details are described for completeness and the major differences in the reanalysis of the raw Raman data taken by Drake et al. [22] earlier and used by Correa et al. [9] and Pope and Correa [13] are discussed. Figure 3 shows a schematic of the experimental arrangement including the tunnel and the Raman diagnostic setup.

A flash-lamp pumped dye laser provides pulses of ~1 J at 488 nm to excite the Raman scattering. The latter is analyzed by a 3/4 m spectrometer with seven photomultiplier tubes at the exit plane and a gated electronic detection system. For each individual pulse, the temperature may be determined by two methods: (a) the Stokes/anti-Stokes N_2 vibrational Raman scattering intensity ratio and (b) the sum of mole fractions of major species assuming ideal gas behavior. The major species (H_2, O_2, H_2O, N_2, CO, CO_2) are determined from their respective Stokes Raman intensities corresponding to each pulse. The temporal resolution (2 μs) of the Raman system is limited by the laser pulse length, the spatial resolution ($0.3 \times 0.3 \times 0.7$ mm^3) by the spectrometer entrance slit and the magnification in the collection optics, and the data acquisition rate (1 Hz) by the laser repetition rate. Most of the Raman data reported here consists of 200-point ensembles.

The data are obtained as follows. The photomultiplier tubes are gated electronically before and

after the firing of the laser. The differential voltages, which correspond to the Raman signal minus the flame background at $t = 0$, are amplified and filtered before digitization using a 14 bit A/D converter. The Raman signals are then corrected for electrical and other background errors corresponding to each channel and are normalized by the laser energy corresponding to the particular shot. The subsequent signals are corrected for relative sensitivities of the photomultiplier tubes to obtain the final value corresponding to the vibrational intensity of Raman scattering (which is linearly proportional to the number density) in the bandpass of the exit slit of the spectrometer. The system was extensively calibrated using 100% pure gases and well-characterized premixed porous-plug burners before these measurements were made.

The correction factors used below were obtained by Drake [26] but not used for previous datasets [22]. In the data reported earlier, the Stokes vibrational Raman scattering intensity from CO_2 was not used directly to determine its mole fraction because of the unknown fraction of total CO_2 vibrational Raman profile in the Raman bandpass measured. The CO_2 mole fraction was instead determined by assuming that the total atomic C/H ratio remained constant in the flame and was equal to the C/H ratio in the fuel. This approach is not entirely satisfactory since it ignores preferential diffusion of hydrogen observed in H_2 jet diffusion flames [25] and does not permit an independent measurement of temperature. To deduce CO_2 directly from the measured Raman intensity the system was calibrated in the system was calibrated in the following manner [26]. A known amount of CO_2 was added to the premixed H_2–air mixture in a laminar–porous plug burner and the resulting Raman bandpass intensity of CO_2 channel was measured. The flame temperature was independently controlled by inserting a series of stainless steel screens upstream of the reaction zone. Thus, the fraction of vibrational spectrum in the Raman bandpass of CO_2 was determined as a function of the temperature.

Another significant improvement in the data was made by correcting for the fraction of Raman signal in the Raman bandpass of the other major species (O_2, N_2, H_2, H_2O, CO) at elevated temperature. This correction factor was inadvertently set to unity in prior analyses of the raw Raman signals. The significance of this correction to the measured Raman signal at elevated temperatures arises from the fact that the Raman exit slits have a finite width due to space limitations and noise considerations; therefore significant portions of the hot Raman bands at higher temperatures do not fall within the finite exit slit and are not measured. The correction factors required to account for the limited Raman spectral bandpass are a function of the species involved, the temperature, the width of the exit slit, and the wavelength region overlapping the physical Raman bandpass. They were calculated by determining the fraction of the predicted Raman vibration band in the Raman bandpass using codes developed by Lapp et al. [27]. Table 1 lists the typical values of the correction factors for the major species involved. As can be seen, the correction factors for H_2 and H_2O are significantly in excess of unity, whereas for CO, O_2, and N_2 they are less than unity. Table 2 compares the typical mean values of temperature, mixture fraction, and mole fractions of major species obtained at $x/d = 25$ in the Re = 8500 syngas flame for two cases: (a) all correction factors set to unity and (b) correction factors allowed to assume their calculated values (listed in

TABLE 1

High Temperature Correction Factors for Vibrational Raman Scattering Used to Correct for the Fraction of Hot Bands of Various Species Falling Outside Their Respective Exit Slits

Temperature (K)	O_2	CO	N_2	H_2O	H_2
300	1.00	1.00	1.00	1.000	1.000
600	.975	.994	1.019	1.001	1.014
900	.914	.966	1.009	1.011	1.060
1200	.848	.922	.982	1.058	1.133
1500	.799	.876	.953	1.141	1.229
1800	.769	.839	.932	1.270	1.345
2100	.756	.812	.922	1.440	1.479
2400	.757	.796	.922	1.650	1.629
2700	.768	.790	.932	1.900	1.795
3000	.787	.792	.950	2.159	1.976

TABLE 2A[a]

Temperature and Mole Fraction of Major Species at $x/d = 25$ Obtained without Correcting for High Temperature Effects (Correction Factors Set to Unity)

Position (r/a)	Temperature (T/2000K)	Mole Fraction						Mixture Fraction	
		CO_2	O_2	CO	N_2	H_2O	H_2	Conv.	Favre
0.63	.600	.084	.007	.233	.489	.105	.075	.443	.448
1.89	.687	.099	.012	.189	.530	.114	.049	.385	.39
3.15	.722	.110	.034	.127	.587	.109	.024	.297	.293
4.39	.647	.101	.084	.054	.655	.090	.008	.199	.176
5.66	.478	.061	.139	.021	.706	.062	.002	.117	.081
6.92	.333	.035	.175	.010	.733	.037	.001	.059	.033
8.18	.229	.017	.194	.004	.757	.019	.001	.023	.011
9.44	.159	.005	.208	.001	.770	.007	0.000	.004	.001
10.69	.146	.004	.209	.001	.772	.004	0.000	.001	.000

[a] 30% H_2, 40% CO, 30% N_2; Re = 8500; $x/d = 25$; correction factors = unity.

Table 1). The mean temperature values are found to be less sensitive to nonunity correction factors since temperature is based upon the sum-of-mole-fraction method, which is not significantly affected by the corrections. However, the mole fractions of some major species including CO, H_2O, and H_2 are found to differ by as much as 20%. The mixture fraction values, which are based on the hydrogen element, are found to increase by as much as 20% due to the increase in the mole fractions of H_2 and H_2O.

COMPARISON

Results of the partial-equilibrium/Monte Carlo model described above were compared with data on the nonpremixed 40% CO, 30% H_2, 30% N_2 "syngas" jet flame in coflowing air. The Raman data for major species, density, and temperature are those of Drake et al. [22] corrected here for high temperature effects as described above. Since these data were taken in radial planes at three axial locations ($x/d = 10$, 25, and 50), the comparisons

TABLE 2B

Temperature and Mole Fractions of Major Species at $x/d = 25$ Corrected for High Temperature Vibrational Bands Using the Correction Factors Listed in Table 1[a]

Position (r/a)	Temperature (T/2000K)	Mole Fraction						Mixture Fraction	
		CO_2	O_2	CO	N_2	H_2O	H_2	Conv.	Favre
0.63	.638	.080	.005	.193	.505	.122	.090	.541	.541
1.89	.739	.093	.007	.144	.545	.141	.062	.504	.506
3.15	.785	.104	.025	.085	.605	.141	.032	.408	.396
4.39	.699	.096	.072	.025	.676	.113	.010	.267	.225
5.66	.504	.059	.129	.004	.725	.072	.003	.145	.093
6.92	.343	.034	.169	0.000	.746	.040	.001	.067	.036
8.18	.231	.016	.191	0.000	.763	.019	.001	.024	.011
9.44	.159	.005	.207	0.000	.771	.007	0.000	.004	.001
10.69	.146	.004	.209	0.000	.773	.004	0.000	.001	.000

[a] a = nozzle radius.

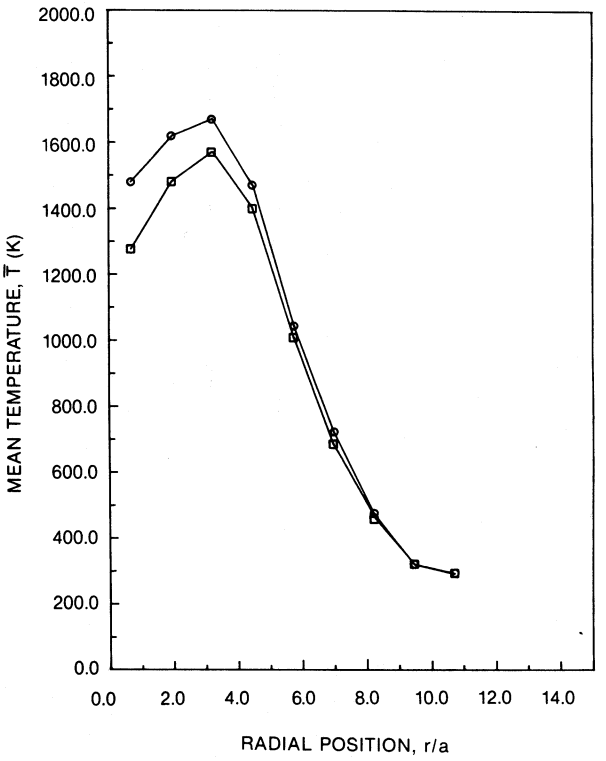

Fig. 4. Comparison of measured radial mean temperature profiles at $x/d = 25$ obtained using two methods: ○, SAS method; □, sum of mole species method.

are made there; $x/d = 50$ corresponds approximately to the visible length of the flame.

As discussed above, the temperature was obtained using two methods: Stokes/anti-Stokes (SAS) ratio and sum-of-mole-fractions. Figure 4 shows the comparison between the mean values of temperature using these two methods at $x/d = 25$. As can be seen, the maximum difference between mean temperatures using the two methods is 200K. The temperature obtained using the SAS method is consistently greater than that obtained using the sum-of-mole-fractions method. For subsequent comparison purposes, the latter method is preferred since the N_2 (AS) Raman signals suffer most from interference due to chemiluminescence in the flame.

Radial profiles of the Favre-averaged mean mixture-fraction ($\tilde{\xi}$) agree quite well at $x/d = 10$ (Fig. 5) except that the jet is predicted to have decayed too slowly on the centerline and to be slightly overspread at the boundary. These differences are made more clear by the mean density profile normalized by that of air (Fig. 5). The central region of the jet is hotter (lower density) than indicated by the data. Temperature profiles (Fig. 6) further confirm this discrepancy and also indicate a difference of about 100K in the off-axis peaks. Nitrogen concentrations plotted in Fig. 6 show better agreement. It should be recalled that the mixture fraction data are based on the measured H_2 and H_2O concentrations.

Some of the other mean major species concentrations are shown in Fig. 7. Compared with the data, CO is underpredicted by 12% at worst, H_2 is overpredicted by about 10%, and CO_2 is overpredicted, which is consistent with a carbon balance. The jet spread is again seen to be slightly overpredicted. The discrepancies in the core are

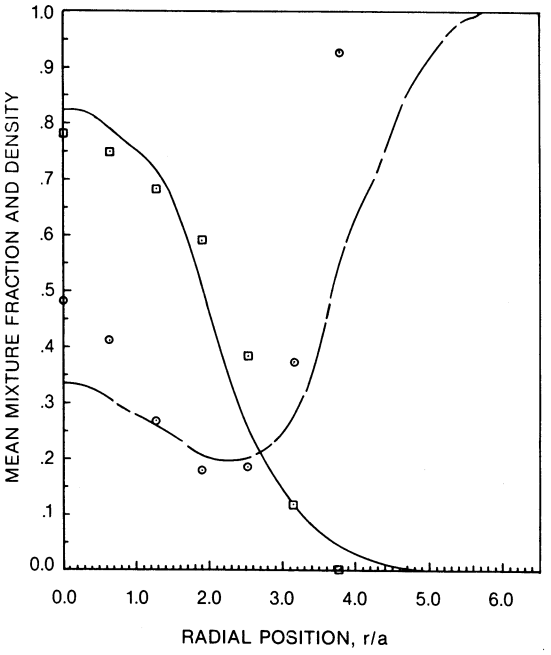

Fig. 5. Mixture fraction $\tilde{\xi}$ and density $\bar{\rho}/\rho_{air}$ at $x/d = 10$: □, $\tilde{\xi}$, ⊙, $\bar{\rho}/\rho_{air}$.

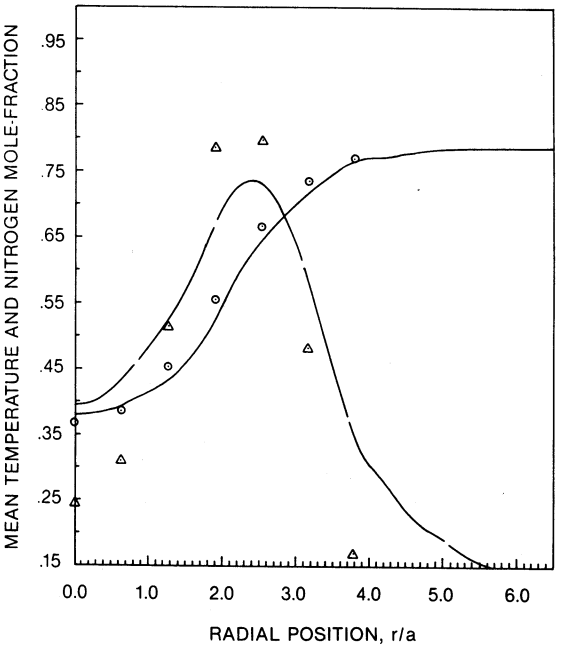

Fig. 6. Temperature $\tilde{T}/2000$K and nitrogen mole-fraction $\tilde{X}_{N_2}$ at $x/d = 10$: △, $\tilde{T}$; ⊙, $\tilde{X}_{N_2}$.

consistent with overpredicting the amount of CO burned and therefore the temperature. The oxygen profiles also appear to agree reasonably well.

Profiles of mean mixture fraction and density at $x/d = 25$ show that the jet spread is predicted quite well but the centerline mixture fraction is about 10% too low (Fig. 8). Correspondingly, since the gas is predicted to be closer to stoichiometric, the temperature is higher by about 150K than measured in the central region (Fig. 9). The spread rate appears quite reasonable. Once again, the nitrogen profiles (Fig. 9) agree well except in the central region, i.e., $r/a < 4$.

Mean major species concentrations at $x/d = 25$ are shown in Fig. 10. The agreement is much better than presented in Pope and Correa [13] because of the changes in the Raman data. Here CO is underpredicted by at worst 10% and O_2, H_2, and CO_2 are predicted very well. The error in CO is more suggestive of an incorrect spread rate than a systematic error which might be attributed to a breakdown of partial equilibrium in the radical-pool.

Mean mixture fraction profiles at $x/d = 50$ show significant disagreement whereas the mean density (Fig. 11) agrees well with the data. Mean temperature and N_2 concentrations also agree fairly well as seen in Fig. 12. The good agreement in N_2 mole fraction is at first glance surprising given the relative lack of agreement in $\tilde{\xi}$. N_2 is essentially an inert species—only trace quantities are converted to NO_x—and therefore should follow a conserved scalar distribution.

This apparent contradiction may be resolved as follows. The measurement of the mole fraction of N_2 is independent of the systematic errors involved in the measurement of other species, whereas the mixture fraction is a derived quantity and is affected by the cumulative errors in measurements of all major species. The instantaneous value of fraction, ξ, can be defined as

$$\xi = \frac{X_{N_2} \Big/ \left(\sum X_i W_i \right)_{\text{mixture}} - X_{N_2}{}^{\text{air}} / W_{\text{air}}}{X_{N_2}{}^{\text{jet}} / W_{\text{jet}} - X_{N_2}{}^{\text{air}} / W_{\text{air}}}, \qquad (7)$$

where X_i and W_i are the mole fraction and molecular weight, respectively, of species i.

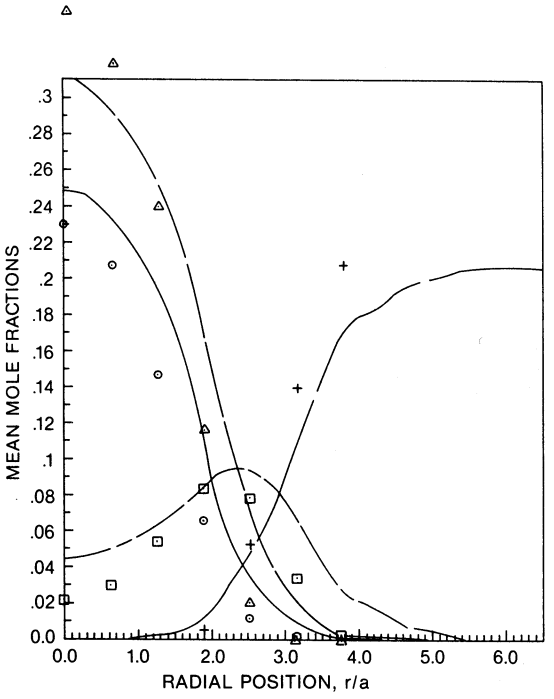

Fig. 7. Major species $\tilde{X}_i$ at $x/d = 10$: ⊙, $\tilde{X}_{H_2}$; △, $\tilde{X}_{CO}$; □, $\tilde{X}_{CO_2}$; +, $\tilde{X}_{O_2}$.

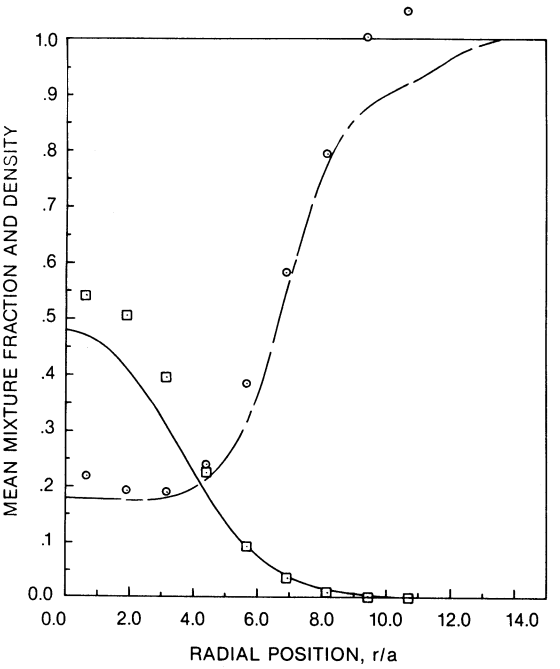

Fig. 8. Mixture fraction $\tilde{\xi}$ and density $\tilde{\rho}/\rho_{air}$ at $x/d = 25$: □, $\tilde{\xi}$; ⊙, $\tilde{\rho}/\rho_{air}$.

Hence, the systematic errors in ξ are due to (a) errors in measurement of all major species and (b) noninclusion of all radicals and other minor species since they are not measured by Raman scattering. These errors affect the "measured" molecular weight $\Sigma X_i W_i$ used in Eq. (7). In fact, a change in mean molecular weight of the gas mixture from 27.86 to 28.8 for the same measured mole fraction of Nitrogen ($X_{N_2} = 0.711$) results in the mixture fraction changing from 0.15 to 0.22. Thus, "measurements" of the mixture fraction are very sensitive to the molecular weight of the mixture especially at low values of $\tilde{\xi}$ (as at $x/d = 50$). It should be noted that all the data for $\tilde{\xi}$ are based on the hydrogen element, but the same argument holds for other definitions since, as Table 3 indicates, the values of $\tilde{\xi}$ based on three elements (C, H, and N) agree well. This result is expected since the effects of differential diffusion, observed in flames at lower Reynolds numbers [25], should be negligible in this relatively high Reynolds number flame. The systematic errors in the measurement of $\tilde{\xi}$ discussed above are common to the three cases.

Mean concentrations of the major species (Fig. 13) at $x/d = 50$ show that there is predicted to be more fuel (CO, H_2), more O_2, and less CO_2 than measured. Assuming no major discrepancy in the predicted mixture fraction, this indicates that the recombination reactions proceed to equilibrium more rapidly than predicted. The spread rate and the level of agreement at the edge are again better than in the central region of the jet.

Prediction of minor species is an important test of the partial-equilibrium model. Comparisons with saturated laser-induced fluorescence data for the mean and rms concentrations of OH were discussed by Correa et al. [9] using the assumed-shape pdf flow model, and by Pope and Correa [13] using the present joint pdf/Monte Carlo flow model. The measurement technique was described by Lucht et al. [28]. While the latter model is in better agreement with the data on rms levels, both showed large superequilibrium concentrations. The agreement between the models and the data is

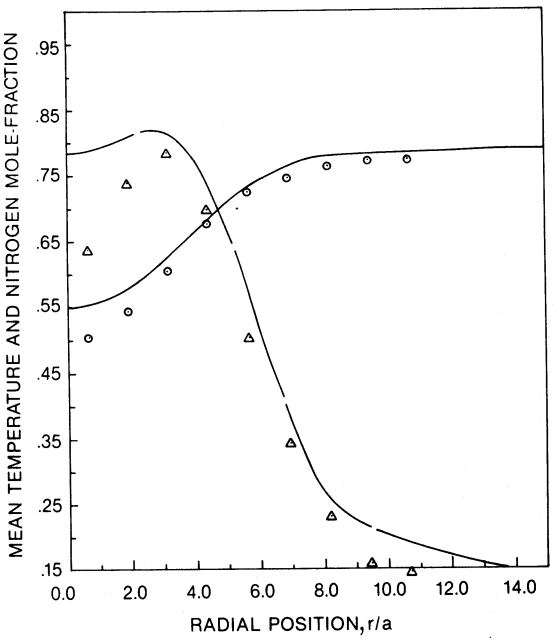

Fig. 9. Temperature $\tilde{T}$/2000K and nitrogen mole-fraction $\tilde{X}_{N_2}$ at $x/d = 25$: △, $\tilde{T}$; ⊙, $\tilde{X}_{N_2}$.

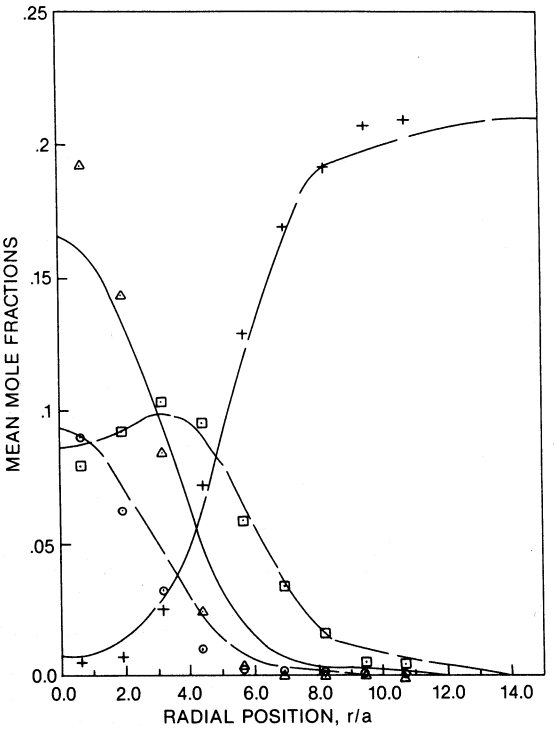

Fig. 10. Major species $\tilde{X}_i$ at $x/d = 25$: ⊙, $\tilde{X}_{H_2}$, △, $\tilde{X}_{CO}$; □, $\tilde{X}_{CO_2}$; +, $\tilde{X}_{O_2}$.

generally within experimental measurement limits except for a consistent difference in the core of the jet at $x/d = 25$, where the OH is substantially overpredicted. This is consistent with the mixture fraction being too low (Fig. 8) and the temperature too high (Fig. 9) in this region.

Instantaneous nonzero concentrations of oxygen in the fuel-rich core of the jet would indicate a lack of full equilibrium. The fast chemistry model explains such observations as nonsimultaneous occurrences of fuel and air (but are not capable of explaining radical overshoot and thermal NO_x); this model could also predict simultaneous nonzero *mean* concentrations of fuel and air, which are apparent in Figs. 7, 10, and 13. Other mechanisms leading to nonzero *mean* concentrations of oxygen in the core are (i) localized extinction due to turbulence and (ii) finite-rate radical pool chemistry as accounted for by the partial-equilibrium model. The first of these may be dismissed in this flame due to the relatively low Reynolds number (8500) and high hydrogen content (30%). In fact, temperature–mixture fraction scattergrams from experiments in a more turbulent flame (Re = 15,000) with less hydrogen in the fuel (40% CO, 10% H_2, 50% N_2) indicate little if any local extinction [29]. Thus finite-rate radical recombination chemistry plays a role in the appearance of oxygen in the core.

CONCLUSIONS

With the addition of two variables to describe the nonequilibrium kinetics and thermochemistry, it appears that finite-rate radical pool kinetics can be predicted with reasonable accuracy in the context of turbulent nonpremixed syngas flames. The model adds the conservation equations for the mixture fraction and a radical-pool reaction progress variable to the hydrodynamic set. In low Mach number flow, the energy can be mapped into the mixture fraction, if equal transport is assumed, because of the negligible contribution of mechanical energy; in high Mach number flow an additional equation for energy is required. This chemi-

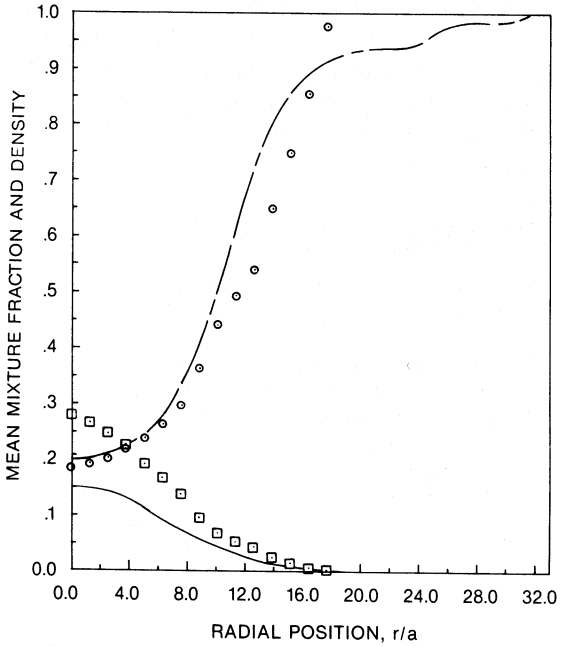

Fig. 11. Mixture fraction $\tilde{\xi}$ and density $\bar{\rho}/\rho_{air}$ at $x/d = 50$: □, $\tilde{\xi}$; ⊙, $\bar{\rho}/\rho_{air}$.

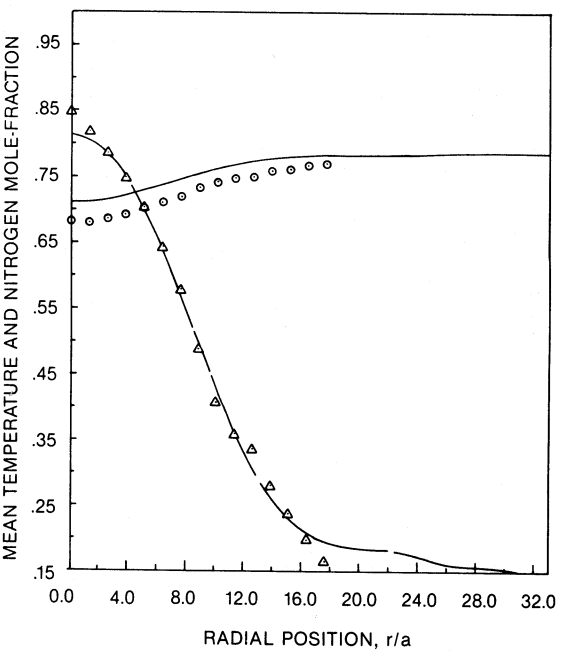

Fig. 12. Temperature $\tilde{T}/2000K$ and nitrogen mole-fraction $\tilde{X}_{N_2}$ at $x/d = 50$: △, $\tilde{T}$; ⊙, $\tilde{X}_{N_2}$.

cal model assumes partial equilibrium in the system, specifically, that the two-body chain-branching and chain-propagating reactions are much faster than any fluid mechanical process and so many be taken as being equilibrated. Radical recombination reactions are treated kinetically.

The joint pdf/Monte Carlo numerical flow model, in which the partial-equilibrium model is implemented, relaxes several of the assumptions made in simpler flow models. In particular, convection including turbulent fluxes are accounted for exactly, as are nonlinear interactions between turbulence and chemical reactions. The shape of the pdf evolves according to a transport equation in which only the pressure fluctuations and molecular transport need to be modeled. Results show better agreement with (reanalyzed) data on major species than that concluded previously.

Calculations were compared with measurements based on Raman scattering of major species, density, temperature, and mixture fraction in a turbulent nonpremixed jet of 40% CO, 30% H_2, and 30% N_2 at a Reynolds number of 8500 burning in coflowing air.

The raw Raman data obtained earlier were reanalyzed with attention to the CO_2 data and the corrections required for high temperature. Mean mole fractions of major species changed by as much as 20%; temperatures were obtained by two methods—Stokes/anti-Stokes intensity ratio for N_2 and the sum-of-mole-fraction—and found to disagree by as much as 200K. Because of the large influence of temperature on H_2 and H_2O vibra-

TABLE 3

Mean Mixture Fraction at $y = 0$ Obtained Based on the Carbon, Hydrogen, and Nitrogen Elements

x/d	Based on N	Based on H	Based on C	Predicted Values
10	0.85	0.78	0.85	0.83
25	0.59	0.54	0.52	0.48
50	0.27	0.28	0.23	0.15

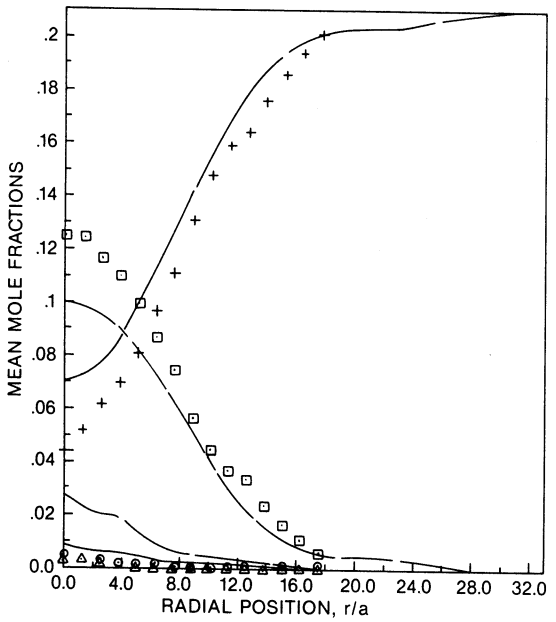

Fig. 13. Major species $\bar{X}_i$ at $x/d = 50$: ⊙, $\bar{X}_{H_2}$; △, $\bar{X}_{CO}$; □, $\bar{X}_{CO_2}$; +, $\bar{X}_{O_2}$.

tional Raman scattering, concentrations of these species are changed and so is too the "measured" mixture fraction, since it is based on these species. A large sensitivity of the "measured" mean mixture fraction to the mean molecular weight was found, particularly when the mean mixture fraction was small.

This study shows that the partial-equilibrium model for the oxyhydrogen radical pool including CO is more useful than was concluded by Correa et al. [9] and Pope and Correa [13]. Although there are discrepancies between the predictions and the data, these are perhaps due to the difficulty of obtaining and interpreting Raman data to a greater extent than previously thought. The reanalyzed data do not show large amounts of CO present where H_2 is absent, which would have been a strong indication of the breakdown of partial equilibrium. Generally good agreement on the minor species (OH) in this flame, where superequilibrium levels are large, further supports the partial-equilibrium model and emphasizes the importance of the relatively slow radical-recombination chemistry [9].

The authors acknowledge the partial support of Dr. Julain Tishkoff (AFOSR Contract No. F49620-85-C-0035) for the experimental portion of this study and the use of the raw Raman data and high-temperature correction factors of Dr. M. C. Drake.

REFERENCES

1. Drake, M. C., Correa, S. M., Pitz, R. W., Shyy, W., and Fenimore, C. P., *Combust. Flame,* 69:347–365 (1987).
2. Correa, S. M., and Mani, R., Paper 87-1961, 21st Joint Propulsion Conference, June, San Diego, CA, 1987.
3. Masri, A. R., and Bilger, R. W., *Twentieth Symposium (International) on Combustion,* The Combustion Institute, Pittsburgh, 1984, pp. 319–326.
4. Tsuji, H., and Yamaoka, I., *Thirteenth Symposium (International) on Combustion,* The Combustion Institute, Pittsburgh, 1984, pp. 319–326.
5. Warnatz, J., *Eighteenth Symposium (International) on Combustion,* The Combustion Institute, Pittsburgh, 1981, pp. 369–384.
6. Iverach, D., Basden, K. S., and Kirov, N. Y., *Fourteenth Symposium (International) on Combustion,* The Combustion Institute, Pittsburgh, (1972), pp. 767–775.
7. Miller, J. A., Kee, R. J., Smooke, M. D., and Grcar, J. F., Paper 84-10, Western States Section of Combustion Institute, 1984.
8. Janicka, J., and Kollman, W., *Seventeenth Symposium (International) on Combustion,* The Combustion Institute, Pittsburgh, 1979, pp. 421–430.
9. Correa, S. M., Drake, M. C., Pitz, R. W., and Shyy, W., Twentieth International Symposium on Combustion, Ann Arbor, 1984.
10. Warnatz, J., *Comb. Sci. Tech.* 26:203–213 (1981).
11. Bilger, R. W., *Comb. Sci. Tech.* 22:251–261 (1980).
12. Fenimore, C. P., and Moore, J., *Combust. Flame* 22:343–351 (1974).
13. Pope, S. B., and Correa, S. M., *Twenty-First Symposium (International) on Combustion,* Munich, FRG, August 1986.
14. Correa, S. M., *Arch. Comb.* 5:223–242 (1986).
15. Kaskan, W. E., *Combust. Flame* 3:49–60 (1959).
16. Bilger, R. W., and Starner, S. H., *Combust. Flame* 51:155–176 (1983).
17. Dixon-Lewis, G., Goldsworthy, F. A., and Greenberg, J. B., *Proceedings Royal Society of London* A346:261–278 (1975).
18. Pope, S. B., Phys. Fluids 24:588–596 (1981).
19. Pope, S. B., *Prog. Energy and Combust. Sci.* 11:119 (1985).
20. Pope, S. B., *AIAA J* 22:896 (1984).
21. Pope, S. B., *Combust. Sci. Technol.* 28:131 (1982).
22. Drake, M. C., Pitz, R. W., Correa, S. M., and Lapp,

M., *Twentieth Symposium (International) on Combustion,* 1984, pp. 327–335.
23. Drake, M. C., Pitz, R. W., Lapp, M., Fenimore, C. P., Lucht, R. P., Sweeney, D. W., and Laurendeau, N. M., *Twentieth Symposium (International) on Combustion,* 1984, pp. 1983–1990.
24. Drake, M. C., Pitz, R. W., and Lapp, M., AIAA Paper No. 84-0544.
25. Drake, M. C., Bilger, R. W., and Starner, S. H., *Nineteenth Symposium (International) on Combustion,* The Combustion Institute, Pittsburgh, 1982, pp. 459–467.
26. Drake, M. C., Report GRI-85/0271, Gas Research Institute, Chicago, 1985.
27. Lapp, M., Drake, M. C., Penney, C. M., Pitz, R. W., and Correa, S. M., General Electric Report 83CRD049, Sept. 1983, DoE Contract DE-AC04-78 ET 13146.
28. Lucht, R. P., Laurendeau, N. M. Sweeney, D. W. Drake, M. C. Lapp, M., and Pitz, R. W., *Optics Letters* 9:90 (1984).
29. Gulati, A., and Correa, S. M., paper 87-1717, 21st Joint Propulsion Conference, San Diego, CA, 1987.

Received 14 April 1987; revised 27 August 1987